The effect of Co doping on antiferromagnetic correlations in the Kondo semi-metal CeNiSn

1996 J. Phys.: Condens. Matter 8 7127

(http://iopscience.iop.org/0953-8984/8/38/015)

J. Phys.: Condens. Matter **8** (1996) 7127–7138. Printed in the UK

The effect of Co doping on antiferromagnetic correlations in the Kondo semi-metal CeNiSn

Taku J Sato†‖, Hiroaki Kadowaki†¶, Hideki Yoshizawa†+, Toshiro Takabatake‡*, Hironobu Fujii‡ and Yosikazu Isikawa§

† Institute for Solid State Physics, University of Tokyo, Roppongi, Minato-ku, Tokyo 106, Japan
‡ Faculty of Integrated Arts and Sciences, Hiroshima University, Higashi-Hiroshima 739, Japan
§ Faculty of Science, Toyama University, Toyama 930, Japan

Received 18 April 1996, in final form 10 July 1996

Abstract. Single-crystal neutron scattering experiments have been performed to study magnetic excitations in $CeNi_{0.9}Co_{0.1}Sn$, in which the pseudo-gap of CeNiSn is suppressed by the doping. In CeNiSn there are two inelastic excitation peaks at $\hbar\omega = 2$ and 4 meV, which correspond to dynamic antiferromagnetic correlations. In $CeNi_{0.9}Co_{0.1}Sn$ the 2 meV peak is smeared out, whereas the 4 meV peak becomes very weak and broad, but preserves the same quasi-one-dimensional character as that for CeNiSn. These results suggest the strong relation between the antiferromagnetic correlations and the pseudo-gap formation.

1. Introduction

Gap formation at the Fermi level is often seen at low temperatures in heavy-fermion or valence-fluctuation compounds, such as CeNiSn [1], CeRhSb [2], $Ce_3Bi_4Pt_3$ [3], SmB_6 [4] and YbB_{12} [5]. Among them, CeNiSn is characterized by a very narrow and anisotropic gap of a few kelvins. Since the narrow gap is thought to originate from strong electron correlations, CeNiSn attracts much attention and has been studied intensively.

Earlier experiments are summarized as follows. CeNiSn crystallizes in the slightly distorted ϵ-TiNiSi-type structure [6], which is illustrated in figure 1. The narrow and anisotropic gap was inferred from many physical properties [1, 7]. For instance, the specific heat divided by temperature (C/T), which increases to $C/T \simeq 0.19$ J mol^{-1} K^{-2} at $T = T_\Delta = 6$ K, abruptly decreases below T_Δ, showing the gap formation below this temperature [8]. The tunnelling conductance also suddenly decreases below T_Δ [9]. At much lower temperatures ($T < 1$ K), (C/T) becomes constant (about 40 mJ mol^{-1} K^{-2}), indicating that the gap formation is not complete and there remains a finite density of states at the Fermi level [7]. Electrical resistivity measurement [10] shows that the gap is anisotropic; that is, it closes at least along the a axis. Since the gap is anisotropic and incomplete, it is called a 'pseudogap'.

There appears another characteristic temperature $T_{coh} > T_\Delta$ in the bulk experiments. For example, the magnetic susceptibility along the easy a axis (χ_a) shows a peak around

‖ Present address: National Research Institute for Metals, Tsukuba, Ibaraki 305, Japan.
¶ Present address: Department of Physics, Tokyo Metropolitan University, Hachioji-shi, Tokyo 192-03, Japan.
+ Present address: Neutron Scattering Laboratory, Institute for Solid State Physics, University of Tokyo, 106-1 Shirakata, Tokai, Ibaraki 319-11, Japan.
* Present address: Faculty of Science, Hiroshima University, Higashi-Hiroshima 739, Japan.

0953-8984/96/387127+12$19.50

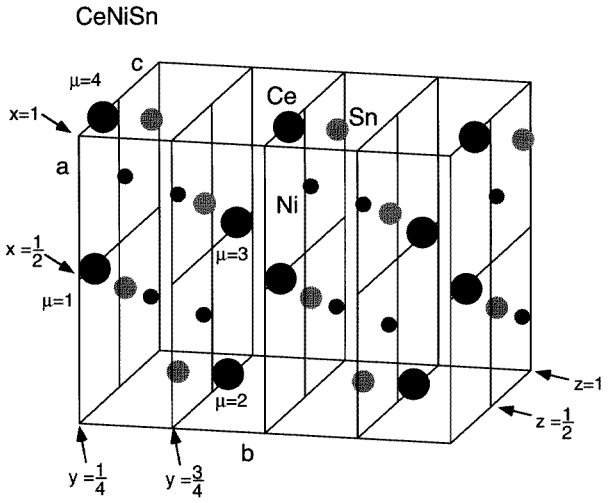

Figure 1. The crystal structure of CeNiSn. Two unit cells along the b axis are drawn. Four Ce positions in the unit cell are represented by $\boldsymbol{d}_\mu$, where $\boldsymbol{d}_1 = (x, \frac{1}{4}, z)$, $\boldsymbol{d}_2 = (\bar{x} + \frac{1}{2}, \frac{3}{4}, z + \frac{1}{2})$, $\boldsymbol{d}_3 = (\bar{x} + 1, \frac{3}{4}, \bar{z} + 1)$ and $\boldsymbol{d}_4 = (x + \frac{1}{2}, \frac{1}{4}, \bar{z} + \frac{1}{2})$ ($x = 0.48, z = 0.20$). Ni and Sn atoms are almost in the same a–c planes, $y \simeq \frac{1}{4}$ or $\frac{3}{4}$.

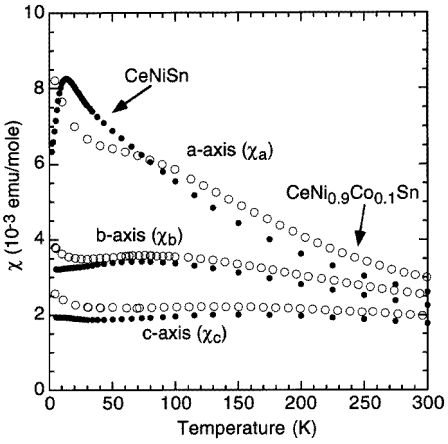

Figure 2. Static susceptibilities along the three directions, χ_a, χ_b and χ_c. The open and closed circles stand for $CeNi_{0.9}Co_{0.1}Sn$ and CeNiSn (after [7]), respectively.

$T_{\rm coh}$ = 12–20 K and decreases below it [7]. This peak behaviour is attributed to the development of antiferromagnetic correlations, namely, the coherence in the Ce lattice. Thus the temperature, $T_{\rm coh}$, is called he 'coherence temperature'. The development of the antiferromagnetic correlations was, in fact, observed in neutron-scattering spectra. From the single-crystal inelastic neutron-scattering experiments [11–13], there appear two inelastic-excitation peaks below $T_{\rm coh}$: $\hbar\omega = 2$ meV, $\boldsymbol{Q} = (0, 1, 0)$ and $(0, 0, 1)$; and $\hbar\omega = 4$ meV, $\boldsymbol{Q} = (Q_a, n + \frac{1}{2}, Q_c)$, where Q_a and Q_c are arbitrary and n is an integer. From the $\boldsymbol{Q}$-dependence, the 2 and 4 meV peaks are regarded as the three-dimensional and quasi-one-

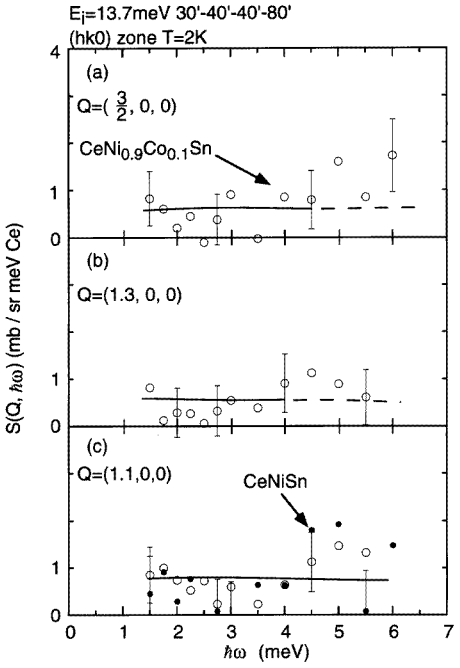

Figure 3. Constant-$\boldsymbol{Q}$ scans on the $\boldsymbol{a}^*$ axis at $\boldsymbol{Q} = (Q_a, 0, 0)$, $Q_a = \frac{3}{2}$, 1.3 and 1.1. The open and closed circles stand for data taken at $T = 2$ K in $CeNi_{0.9}Co_{0.1}Sn$ and CeNiSn [13], respectively. The broken line represents the magnetic contribution from which the phonon scattering has been subtracted. The full line is a guide for the eye.

dimensional dynamic antiferromagnetic correlations, respectively. (The former (0,1,0) and (0,0,1) are forbidden nuclear reflections, and thus are also antiferromagnetic in nature [11].) Since the pseudo-gap formation takes place in the temperature region within which the antiferromagnetic correlations are well developed, it is desired to clarify the relation between the antiferromagnetic correlations and the pseudo-gap formation.

The pseudo-gap in CeNiSn is known to be sensitive to substitutions in the Ni sublattice: substitutions of small amounts of Cu, Pt and Co at the Ni sites suppress the pseudo-gap [1]. Among them, the Co-doped system has been widely studied with polycrystalline samples by measuring the specific heat [1], magnetic susceptibility [14], high-field magnetization [14], and nuclear spin relaxation ratio, $1/T_1$, of NMR [15]. The suppression of the pseudo-gap is most apparently evident from the NMR measurement, in which $1/T_1$ follows the Korringa law at low temperatures such as $T < 10$ K in the 10% Co-doped sample. The specific heat divided by temperature, C/T, at low temperature becomes rather small and its behaviour rather flat (about 0.1 J mol^{-1} K^{-2} for a 10 sample). These results indicate that the system becomes valence-fluctuating and metallic. The magnetic susceptibility and high-field magnetization also become small, confirming the valence-fluctuating character and the absence of the magnetic anomaly at low temperatures.

In this work, we have performed the neutron inelastic-scattering experiments in pseudo-gap-suppressed $CeNi_{0.9}Co_{0.1}Sn$. Our aim is to clarify the variation of the dynamic antiferromagnetic correlations in the pure and doped samples. This will enable us to experimentally reveal the relation between the pseudo-gap formation and the dynamic

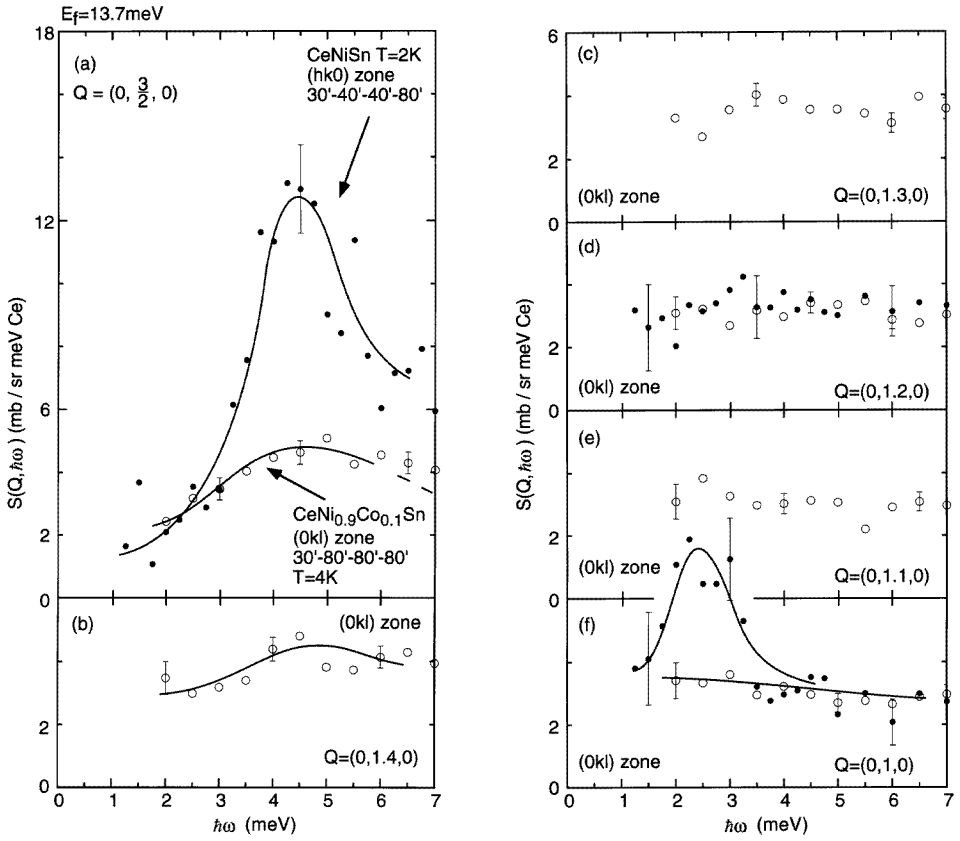

Figure 4. Constant-$\boldsymbol{Q}$ scans on the b^*axis at $\boldsymbol{Q} = (0, Q_b, 0)$, $Q_b = \frac{3}{2}$, 1.4, 1.3, 1.2, 1.1 and 1. Open circles stand for the data taken in $CeNi_{0.9}Co_{0.1}Sn$ at $T = 4$ K, whereas the closed circles stand for data taken in CeNiSn [13] at $T = 2$ K. The broken line represents the phonon-subtracted magnetic contribution. The full line is a guide for the eye.

antiferromagnetic correlations. The excitation spectra in pure CeNiSn were reported in the previous study [13] and a few selected CeNiSn spectra will be reproduced for comparison. Part of this report was published earlier [16].

2. The experimental procedure

A single crystal of $CeNi_{0.9}Co_{0.1}Sn$ was grown by the Czochralski method using a tungsten crucible under an argon gas atmosphere of 5–10 Torr. The pulling speed was 10 mm h^{-1} and the rotation speed 5 rpm. The purities of the starting materials Ce, Ni, Co and Sn were 99.99%, 99.998%, 99.998% and 99.999%, respectively. Details of the crystal growth were reported in [17]. The volume of the $CeNi_{0.9}Co_{0.1}Sn$ single crystal was 1.7 cm^3.

Inelastic neutron-scattering experiments were performed on the ISSP triple-axis spectrometer GPTAS installed at JRR-3M JAERI (Tokai). Pyrolytic graphite (002) reflections were used for the vertically focusing monochromator and analyser. Neutrons with a second-order wavelength were removed by a pyrolytic graphite filter. The experiments were carried out either in the E_i- or in the E_f-fixed mode with the fixed energy of 13.7 meV.

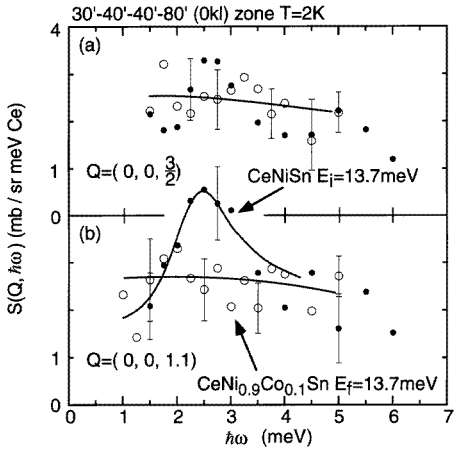

Figure 5. Constant-$\boldsymbol{Q}$ scans on the c^* axis at $\boldsymbol{Q} = (0, 0, Q_c)$, $Q_c = \frac{3}{2}$ and 1.1. The open and closed circles stand for data taken at $T = 2$ K in $CeNi_{0.9}Co_{0.1}Sn$ and CeNiSn [13], respectively. The full line is a guide for the eye.

Collimations of 30'–40'–40'–80' or 30'–80'–80'–80' were employed. These configurations give the energy resolutions at the elastic position as $\Delta\hbar\omega = 0.9$ meV for 30'–40'–40'–80' and $\Delta\hbar\omega = 1.3$ meV for 30'–80'–80'–80' in full width at half maximum. The sample was mounted in a closed cycle ^{4}He refrigerator or the Orange cryostat with the [100] or [001] direction vertical, so as to measure the scattering in the $(0, k, l)$ or $(h, k, 0)$ plane.

Inelastic neutron-scattering spectra were corrected for background and absorption, and were scaled to absolute units of cross section [13]. They are given as the scattering function $S(\boldsymbol{Q}, \hbar\omega) = (k_i/k_f)(d^2\sigma/d\Omega dE_f)$. The absorption was corrected by numerically calculating the absorption factors. The scattering intensity was converted to absolute units by a calibration using the calculated and observed intensities of the acoustic phonons of the standard copper crystal and CeNiSn. For the background correction, we considered the following possibilities: (i) scattering by air, the cryostat and the sample holder; (ii) a tail of the incoherent elastic scattering; (iii) the incoherent inelastic scattering by the phonon; and (iv) double scattering due to the coherent phonon and the incoherent elastic scattering. The background (i) was estimated by measuring the scattering intensity without the sample and (ii) was measured using a vanadium standard. The backgrounds (iii) and (iv) were numerically calculated and found to be negligible at low temperatures, such as $T = 4$ K. After the correction, we think that the spectra contain the magnetic excitation and coherent inelastic scattering by the phonon.

The phonon scattering appears as peaks in the excitation spectra. We distinguished the phonon peaks from the magnetic excitation by measuring the spectra at room temperature. This procedure utilizes the large temperature dependence of the phonon intensity, which follows the Bose factor, $1 + n(\hbar\omega) = 1/(1 - e^{-\beta\hbar\omega})$, where $\beta = 1/(k_B T)$. We found that the peaks appear at $\hbar\omega > 5$ meV for the $\boldsymbol{Q}$ range of the present study and thus do not seriously contaminate the low-energy magnetic excitation. Furthermore, using the temperature-dependence, phonon contamination at low temperatures can be roughly estimated from the spectra at room temperature. We subtracted the estimated contamination from the spectra containing the phonon peak and obtained magnetic contributions, which will be presented by broken lines in following figures.

3. Experimental results

3.1. Static susceptibility

The static susceptibilities, χ_α ($\alpha = a, b, c$), of the single-crystalline CeNiSn and $CeNi_{0.9}Co_{0.1}Sn$ are shown in figure 2. The data for CeNiSn are reproduced from [7]. Those for $CeNi_{0.9}Co_{0.1}Sn$ were taken in the present study using a vibrating sample magnetometer under the magnetic field of $H = 1$ T. As seen from figure 2, χ_α in the two samples are almost the same for all the directions, except for the rapid increase in $CeNi_{0.9}Co_{0.1}Sn$ at low temperatures. Since no magnetic anomaly was reported in the polycrystalline sample at low temperatures [14], this increase can possibly be attributed to the impurity contamination and thus is not intrinsic. The similar values of χ_α suggest that the anisotropy is not changed by the doping, namely $\chi_a > \chi_b > \chi_c$. A difference between CeNiSn and $CeNi_{0.9}Co_{0.1}Sn$ appears in the temperature variation of χ_a around T_{coh}: the peak behaviour, observed in CeNiSn, cannot be seen in $CeNi_{0.9}Co_{0.1}Sn$. Since the peak behaviour can be attributed to the development of the antiferromagnetic correlations, this suggests that the antiferromagnetic correlations are suppressed by the doping.

3.2. Inelastic excitation spectra on the reciprocal lattice axes: anisotropy of the magnetic fluctuation

The scattering function on the three reciprocal lattice axes is related to the diagonal terms of the generalized susceptibility, $\mathrm{Im}\chi^{\alpha\alpha}(\boldsymbol{Q}, \hbar\omega)$, as

$$S(\boldsymbol{Q}, \hbar\omega) = \frac{(\gamma r_0)^2 V}{(2\mu_B)^2 \pi} \frac{1}{(1 - \mathrm{e}^{-\beta\hbar\omega})} \sum_\alpha \left(1 - \hat{Q}_\alpha^2\right) \mathrm{Im}\left[\chi^{\alpha\alpha}(\boldsymbol{Q}, \hbar\omega)\right] \tag{1}$$

where γ, r_0, V and μ_B are the gyromagnetic ratio of a neutron, the classical electron radius, the volume of the sample and the Bohr magneton [13, 18]. The unit scattering vector $\hat{\boldsymbol{Q}}$ is defined as $\hat{\boldsymbol{Q}} = \boldsymbol{Q}/Q$. To investigate the diagonal terms first, we observed the spectra on the reciprocal lattice axes. Shown in figures 3–and 5 are several constant-$\boldsymbol{Q}$ scans observed in $CeNi_{0.9}Co_{0.1}Sn$ on the $\boldsymbol{a}^*$, $\boldsymbol{b}^*$ and $\boldsymbol{c}^*$ axes, which correspond to $\mathrm{Im}[\chi^{bb}(\boldsymbol{Q}, \hbar\omega) + \chi^{cc}(\boldsymbol{Q}, \hbar\omega)]$, $\mathrm{Im}[\chi^{cc}(\boldsymbol{Q}, \hbar\omega) + \chi^{aa}(\boldsymbol{Q}, \hbar\omega)]$ and $\mathrm{Im}[\chi^{aa}(\boldsymbol{Q}, \hbar\omega) + \chi^{bb}(\boldsymbol{Q}, \hbar\omega)]$, respectively. We also plot the spectra in CeNiSn observed at a few selected $\boldsymbol{Q}$ positions for comparison.

From figures 3–5, one finds that the scattering intensity on the $\boldsymbol{a}^*$ axis is much smaller than those on the $\boldsymbol{b}^*$ and $\boldsymbol{c}^*$ axes. It can be shown that each diagonal term, $\mathrm{Im}\chi^{\alpha\alpha}(\boldsymbol{Q}, \hbar\omega)$, is positive for positive $\hbar\omega$. Thus, if the $\boldsymbol{Q}$-dependence of the magnetic excitation is neglected, this result means that $\mathrm{Im}\chi^{bb}(\boldsymbol{Q}, \hbar\omega), \mathrm{Im}\chi^{cc}(\boldsymbol{Q}, \hbar\omega) \ll \mathrm{Im}\chi^{aa}(\boldsymbol{Q}, \hbar\omega)$. Namely, the low-energy magnetic fluctuation is restricted along the a axis. In addition, the scattering intensity in $CeNi_{0.9}Co_{0.1}Sn$ is almost the same as that in CeNiSn for each $\boldsymbol{Q}$ position except for the positions where the inelastic peaks were observed. Thus we can conclude that the anisotropy of the low-energy magnetic fluctuation is not changed by the doping. This result is consistent with the anisotropy of the static susceptibility.

3.3. Suppression of the inelastic excitation peaks

Figures 4(f) and 5(b) show the constant-$\boldsymbol{Q}$ scans of $CeNi_{0.9}Co_{0.1}Sn$ at $\boldsymbol{Q} = (0, 1, 0)$ and $T = 4$ K, and at $\boldsymbol{Q} = (0, 0, 1.1)$ and $T = 2$ K, respectively. By comparing them with the spectra of CeNiSn at $T = 2$ K, also shown in figures 4 and 5, one finds that the 2 meV peak is suppressed in $CeNi_{0.9}Co_{0.1}Sn$. Figure 4(a) shows the constant-$\boldsymbol{Q}$ scans at $\boldsymbol{Q} = (0, \frac{3}{2}, 0)$ for CeNiSn ($T = 2$ K) and $CeNi_{0.9}Co_{0.1}Sn$ ($T = 4$ K). The 4 meV excitation peak is also

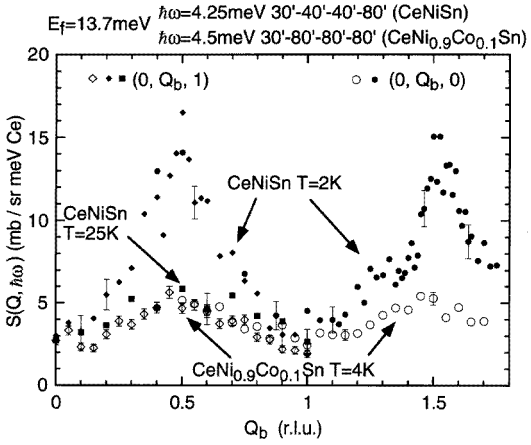

Figure 6. Constant-E scans along $\boldsymbol{Q} = (0, Q_b, 0)$ (circles) and $\boldsymbol{Q} = (0, Q_b, 1)$ (diamonds and squares). Filled symbols stand for the scans in CeNiSn at $\hbar\omega = 4.25$ meV, at $T = 2$ K (diamonds and circles) and $T = 25$ K (squares) [13]. Open symbols stand for the scans in $CeNi_{0.9}Co_{0.1}Sn$ at $\hbar\omega = 4.5$ meV and $T = 4$ K.

suppressed by the doping. However, the suppression of the 4 meV peak is not complete and there remains a broad and weak peak. The Q_b-dependence of the broad and weak 4 meV peak is also shown in figure 4. Apart from $Q_b = \frac{3}{2}$, the peak disappears and the spectrum becomes rather flat. To confirm this Q_b-dependence, we performed constant-E scans along $\boldsymbol{Q} = (0, Q_b, 0)$ and $\boldsymbol{Q} = (0, Q_b, 1)$, at $\hbar\omega = 4.5$ meV and $T = 4$ K. The resulting scans are shown in figure 6. The scans for CeNiSn at $\hbar\omega = 4.25$ meV, at $T = 2$ and 25 K are also shown in figure 6 for comparison. The scans for $CeNi_{0.9}Co_{0.1}Sn$ apparently show two peaks at $Q_b = n + \frac{1}{2}$. Since the peak positions along the Q_b direction are exactly the same as those for CeNiSn, we can conclude that the weak and broad 4 meV peak, observed in the constant-$\boldsymbol{Q}$ scan at $\boldsymbol{Q} = (0, \frac{3}{2}, 0)$, is a reminiscent of the sharp 4 meV peak for pure CeNiSn. The peak becomes broad in the Q_b direction, indicating that the correlation length becomes shorter: the correlation length in $CeNi_{0.9}Co_{0.1}Sn$ is estimated as $\xi_b = 0.4b$ Å, which is about a half of that deduced in CeNiSn. From the above results, we can conclude that the corresponding antiferromagnetic correlations are suppressed, but still remain at least for $\hbar\omega = 4$ meV. Note that the constant-E scan for $CeNi_{0.9}Co_{0.1}Sn$ at $T = 4$ K is almost the same as that for CeNiSn at $T = 25$ K (see figure 6). This suggests that the doping has an effect similar to that of rising temperature on the antiferromagnetic correlations.

3.4. Anisotropy and dimensionality of the dynamic antiferromagnetic correlation

To investigate the Q_c- and Q_a-dependences of the 4 meV peak for $CeNi_{0.9}Co_{0.1}Sn$, we performed constant-$\boldsymbol{Q}$ scans at $\boldsymbol{Q} = (0, \frac{3}{2}, Q_c)$ and $(Q_a, \frac{3}{2}, 0)$ (Q_a, $Q_c = \frac{1}{4}, \frac{1}{2}, \frac{3}{4}$ and 1). The results are shown in figures 7 and 8, respectively. As shown in figures 7 and 8, the spectra at $Q_c \neq 0$ (figure 7) and at $Q_a \neq 0$ (figure 8) are almost the same as that at $\boldsymbol{Q} = (0, \frac{3}{2}, 0)$. To confirm these Q_a- and Q_c-dependences, we performed constant-E scans over a wide $\boldsymbol{Q}$ range in addition to the region investigated by the constant-$\boldsymbol{Q}$ scans. The reason that we measured the wide $\boldsymbol{Q}$ range is that $S(\boldsymbol{Q}, \hbar\omega)$ and hence $\mathrm{Im}\chi^{\alpha\alpha}(\boldsymbol{Q}, \hbar\omega)$ are not necessarily periodic functions with periods $\boldsymbol{a}^*$, $\boldsymbol{b}^*$ and $\boldsymbol{c}^*$ [13]. The constant-E scan along the Q_c direction in $CeNi_{0.9}Co_{0.1}Sn$ ($T = 4$ K) is shown in figure 9, together with

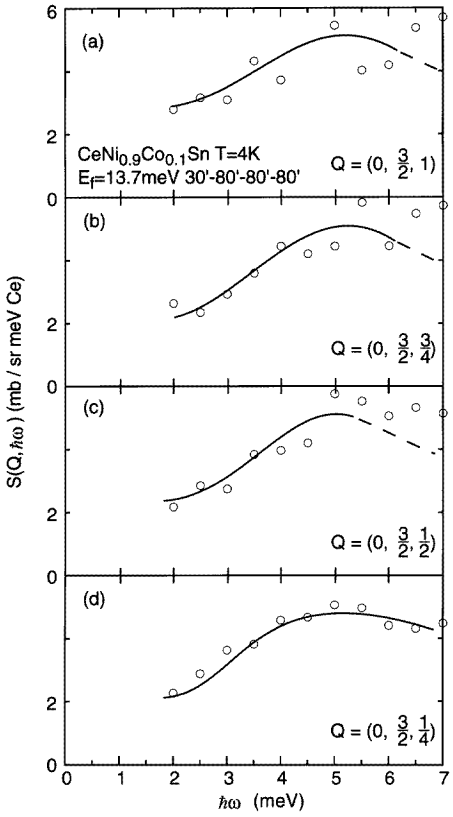

Figure 7. Constant-$\boldsymbol{Q}$ scans at $\boldsymbol{Q} = (0, \frac{3}{2}, Q_c)$, $Q_c = 1, \frac{3}{4}, \frac{1}{2}$ and $\frac{1}{4}$ in $CeNi_{0.9}Co_{0.1}Sn$, at $T = 4$ K. The broken and full lines are the phonon-subtracted magnetic contribution and a guide for the eye, respectively.

the corresponding data in CeNiSn ($T = 2$ K). The Q_c-dependence in the two samples is almost the same and is well approximated by the square of the form factor of Ce^{3+} [19], $f(\boldsymbol{Q})^2$, which is shown by the full line in figure 9. The Q_a-dependence for CeNiSn and $CeNi_{0.9}Co_{0.1}Sn$, shown in figure 10, is also the same: it shows a rapid decrease at large Q_a and is well approximated by $f(\boldsymbol{Q})^2(1-\hat{Q}_a^2)$ (dotted line), where $(1-\hat{Q}_a^2)$ is the orientational factor of $\mathrm{Im}\chi^{aa}(\boldsymbol{Q}, \bar{h}\omega)$. Except for the orientational factor and form factor, the scattering function along Q_a and Q_c is almost constant; that is, the 4 meV peak can be observed for arbitrary Q_a and Q_c. As already shown in figure 6, the constant-E scans along the $\boldsymbol{b}^*$ axis in CeNiSn and $CeNi_{0.9}Co_{0.1}Sn$ show the same Q_b-dependence except for the intensity and peak width. Since the $\boldsymbol{Q}$-dependence in CeNiSn and $CeNi_{0.9}Co_{0.1}Sn$ is the same for each Q_a, Q_b or Q_c direction, the dynamic antiferromagnetic correlation with $\bar{h}\omega = 4$ meV in $CeNi_{0.9}Co_{0.1}Sn$ has the same characteristics as those deduced in CeNiSn [13]. These are summarized as follows: (i) the polarization of the fluctuation is along the a axis, that is, $\mathrm{Im}\chi^{aa}(\boldsymbol{Q}, \bar{h}\omega)$; and (ii) the antiferromagnetic correlation is quasi-one-dimensional along the b axis and only exists between the moments that are related through the translational symmetry operations. The real-space spin-configuration of the antiferromagnetic correlation is also the same as that deduced in CeNiSn, which is depicted in figure 11 by reproducing from figure 17(a) of [13]. These results show that the dimensionality and anisotropy of the

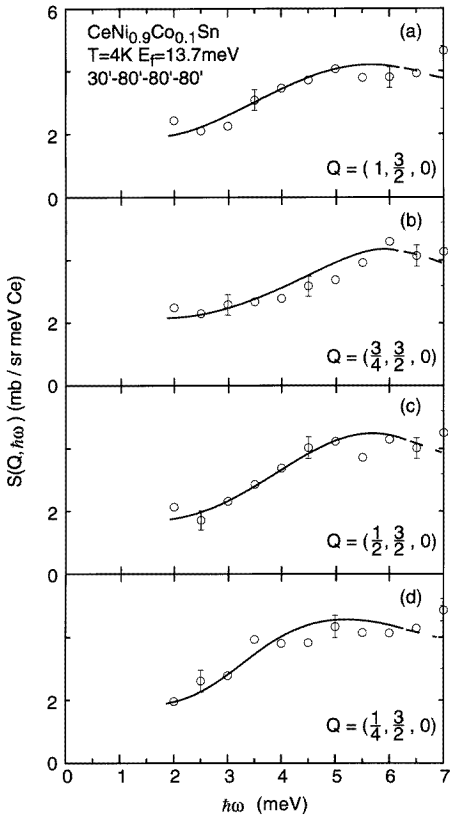

Figure 8. Constant-$\boldsymbol{Q}$ scans at $\boldsymbol{Q} = (Q_a, \frac{3}{2}, 0)$, $Q_a = 1, \frac{3}{4}, \frac{1}{2}$ and $\frac{1}{4}$ in $CeNi_{0.9}Co_{0.1}Sn$, at $T = 4$ K. The broken and full lines are the phonon-subtracted magnetic contribution and a guide for the eye, respectively.

4 meV antiferromagnetic correlation are not changed by the doping.

4. Discussion and conclusions

The most pronounced result that we observed in the present study is the suppression of the antiferromagnetic correlations by the Co doping: the 2 meV peak disappears within our experimental accuracy, whereas the 4 meV peak becomes very weak and broad. Since there exists no quantitative theory that describes the effect of Co doping on the antiferromagnetic correlations in CeNiSn so far, we will briefly discuss it qualitatively.

The photoemission study showed that the Ni 3d band is located close to the Fermi level and hybridizes with the conduction electron band, which consists mainly of the Sn 5p states [20]. Thus the doping with Co impurities decreases the conduction electron number and results in lowering of the Fermi level, ϵ_{F}, towards the Ce 4f level, ϵ_f. Since the Kondo temperature, T_{K}, is proportional to $\exp[-(\epsilon_{\mathrm{F}} - \epsilon_f)]$, the Co doping will strongly enhance T_{K} [14]. As a result, the magnetic moments of Ce are rather quenched via single-site Kondo fluctuation at higher temperatures and the system becomes a valence-fluctuating one. Then even at low temperatures the single-site Kondo fluctuation prevails and the

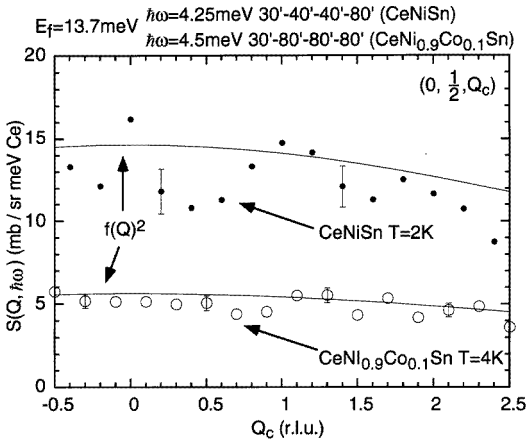

Figure 9. Constant-E scans along $\boldsymbol{Q} = (0, \frac{1}{2}, Q_c)$. Closed circles stand for the scan in CeNiSn at $\hbar\omega = 4.25$ meV and $T = 2$ K [13], whereas open circles stand for the scan in $CeNi_{0.9}Co_{0.1}Sn$ at $\hbar\omega = 4.5$ meV and $T = 4$ K. The full line stands for the square of the form factor, $f(\boldsymbol{Q})^2$ [19].

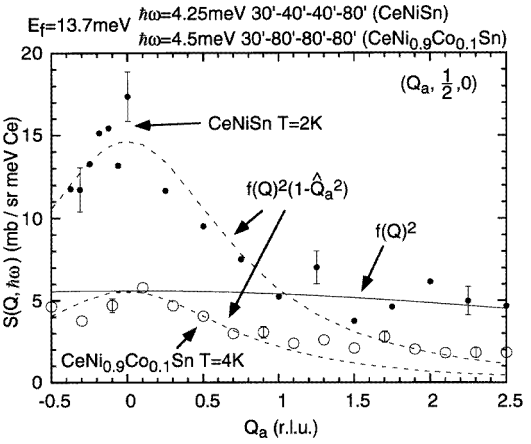

Figure 10. Constant-E scans along $\boldsymbol{Q} = (Q_a, \frac{1}{2}, 0)$. Closed circles stand for the scan in CeNiSn at $\hbar\omega = 4.25$ meV and $T = 2$ K [13], whereas open circles stand for the scan in $CeNi_{0.9}Co_{0.1}Sn$ at $\hbar\omega = 4.5$ meV and $T = 4$ K. The dotted and full lines stand for $f(\boldsymbol{Q})^2(1 - \hat{Q}_a^2)$ and $f(\boldsymbol{Q})^2$, respectively, where $f(\boldsymbol{Q})$ is the form factor [19] and $(1 - \hat{Q}_a^2)$ the orientational factor of $\mathrm{Im}\chi^{aa}(\boldsymbol{Q}, \hbar\omega)$.

antiferromagnetic correlations cannot develop. In addition to the effect described above, the Co impurities also behave as impurity scatterers and introduce randomness into the periodic lattice. These scatterers will destroy the coherence in the ground state, which may also suppress the antiferromagnetic correlations in the Ce lattice. However, since the anisotropy and dimensionality of the magnetic fluctuation are almost unchanged in the Co doped system, it is suggested that the ligand field around Ce is not strongly affected by the doping. This implies that the potentials produced by the Ni and Co atoms in $CeNi_{0.9}Co_{0.1}Sn$ are similar. In this case the periodicity of the potentials may not be strongly destroyed. Thus the dominant origin of the suppression of the antiferromagnetic correlations may possibly

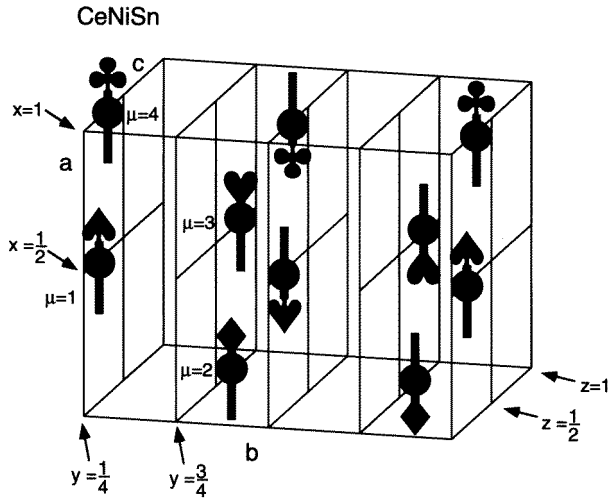

Figure 11. A schematic illustration of the real-space antiferromagnetic correlation of the 4 meV excitation. Magnetic moments are drawn as arrows. Closed circles indicate four Ce positions in the unit cell. The definition of μ is given in the caption of figure 1. Moments of the same arrow couple antiferromagnetically along the b axis. Moments of the different arrows have no correlation to each other. This illustration is reproduced from [13].

be the change in the conduction electron number.

In conclusion, the effect of the partial substitution of Co for Ni on the magnetic excitations in CeNiSn was investigated in the energy range 2–7 meV by performing neutron-scattering measurements on the single-crystalline $CeNi_{0.9}Co_{0.1}Sn$. The low-energy magnetic fluctuation is dominated by the easy a axis component, $\mathrm{Im}\chi^{aa}(\boldsymbol{Q}, \hbar\omega)$, and the anisotropy shows little variation with the doping. On the other hand, the inelastic excitation peaks at $\hbar\omega = 2$ and 4 meV, observed in pure CeNiSn, are strongly suppressed in $CeNi_{0.9}Co_{0.1}Sn$. Since the peaks are regarded as the dynamic antiferromagnetic correlations, this result suggests the strong relation between the pseudo-gap formation and the dynamic antiferromagnetic correlations. The former 2 meV peak is suppressed within our experimental accuracy, whereas the suppression of the latter 4 meV peak is not complete and there remains a weak and broad peak around 4 meV. The $\boldsymbol{Q}$-dependence of the remaining peak was carefully investigated. As a result, we found that the corresponding dynamic antiferromagnetic correlation is quasi-one-dimensional and its polarization is along the easy a axis, which are the same as those in pure CeNiSn. The effect of the doping on the dynamic antiferromagnetic correlation appears only in the shorter correlation length and broader line width, not in the anisotropy and dimensionality.

Acknowledgments

The authors would like to thank G Nakamoto for valuable discussions. One of the authors (TT) thanks the Yamada Science Foundation for financial support.

References

[1] Takabatake T, Nakazawa Y and Ishikawa M 1987 *Japan. J. Appl. Phys.* **26** suppl. 3 547

Takabatake T and Fujii H 1993 *Japan. J. Appl. Phys.* **8** 254
Takabatake T, Nakamoto G, Tanaka H, Bando Y, Fujii H, Nishigori S, Goshima H, Suzuki T, Fujita T, Oguro I, Hiraoka T and Malik S K 1994 *Physica* B **199 & 200** 457
[2] Malik S K and Adroja D T 1991 *Phys. Rev.* B **43** 6277
[3] Hundley M F, Canfield P C, Thompson J D, Fisk Z, Lawrence J M 1990 *Phys. Rev.* B **42** 6842
Bucher B, Schlesinger Z, Canfield P C and Fisk Z 1994 *Phys. Rev. Lett.* **72** 522
[4] Allen J W, Batlogg B and Wachter P 1979 *Phys. Rev.* B **20** 4807
[5] Kasaya M, Iga F, Takigawa M and Kasuya T 1985 *J. Magn. Magn. Mater.* **47 & 48** 429
[6] Higashi I, Kobayashi K, Takabatake T and Kasaya M 1993 *J. Alloys Compounds* **193** 300
[7] Takabatake T, Nakamoto G, Yoshino T, Fujii H, Izawa K, Nishigori S, Goshima H, Suzuki T, Fujita T, Maezawa K, Hiraoka T, Okayama Y, Oguro I, Menovsky A A, Neumaier K, Brückl A and Andres K 1996 *Physica* B at press
[8] Nishigori S, Goshima H, Suzuki T, Fujita T, Nakamoto G, Takabatake T, Fujii H and Sakurai J 1993 *Physica* B **186–188** 406
[9] Ekino T, Takabatake T, Tanaka H and Fujii H 1995 *Phys. Rev. Lett.* **75** 4262
[10] Nakamoto G, Takabatake T, Bando Y, Fujii H, Izawa K, Suzuki T, Fujita T, Minami A, Oguro I, Tai L T and Menovsky A A 196 *Physica* B **206–207** 840
Nakamoto G, Takabatake T, Fujii H, Minami A, Maezawa K, Oguro I and Menovsky A A 1995 *J. Phys. Soc. Japan* **64** 4834
[11] Mason T E, Aeppli G, Ramirez A P, Clausen K N, Broholm C, Stücheli N, Bucher E and Palstra T T M 1992 *Phys. Rev. Lett.* **69** 490
[12] Kadowaki H, Sato T, Yoshizawa H, Ekino T, Takabatake T, Fujii H, Regnault L P and Isikawa Y 1994 *J. Phys. Soc. Japan* **63** 2074
[13] Sato T J, Kadowaki H, Yoshizawa H, Ekino T, Takabatake T, Fujii H, Regnault L P and Isikawa Y 1995 *J. Phys.: Condens. Matter* **7** 8009
[14] Takabatake T, Nakamoto G, Tanaka H, Fujii H, Nishigori S, Suzuki T, Fujita T, Ishikawa M, Oguro I, Kurisu M and Menovsky A A 1994 *Proc. Hiroshima Workshop on Transport and Thermal Properties of f-electron Systems* ed H Fujii *et al* (New York: Plenum)
[15] Nakamura K, Kitaoka Y, Asayama K, Takabatake T, Nakamoto G, Tanaka H and Fujii H 1996 *Phys. Rev.* B **53** 6385
[16] Sato T J, Kadowaki H, Yoshizawa H, Nakamoto G, Ekino T, Takabatake T, Fujii H, Regnault L P and Isikawa Y 1996 *Physica* B at press
[17] Isikawa Y, Mori K, Ogisi Y, Oyaba K and Sato K 1991 *J. Phys. Soc. Japan* **60** 2514
[18] Lovesey S W 1984 *Theory of Neutron Scattering From Condensed Matter* (Oxford: Clarendon)
[19] Blume M, Freeman A J and Watson R E 1962 *J. Chem. Phys.* **37** 1245
[20] Nohara S, Namatame H, Fujimori A and Takabatake T 1993 *Physica* B **186–188** 403
Nohara S, Namatame H, Fujimori A and Takabatake T 1993 *Phys. Rev.* B **47** 1754